Optical singularities in plasmonic fields near single subwavelength holes

A de Hoogh, N Rotenberg, and L Kuipers

FOM Institute AMOLF, Science Park 104, 1098 XG Amsterdam, The Netherlands

Abstract

We identify phase and polarization singularities in near-field measurements and theoretical modeling of the electric near field distributions that result from the scattering of surface plasmon polaritons from single subwavelength holes in optically thick gold films. We discuss properties of the singularities, such as their topological charge or the field amplitudes at their locations. We show that it is possible to tune the in-plane field amplitude at the positions of the polarization singularities by 3 orders of magnitude simply by varying the hole or incident plasmon beam size.

Keywords

Optical singularities, nanoplasmonic, near-fields

PACS Numbers: 42.25.Fx, 73.20.Mf, 73.50.Bk

1. Introduction

The creation of structured light fields that can carry angular momentum is a topic of intense research. In the far-field beams can carry either spin or orbital angular momentum, as is the case for, for example, vortex or circularly polarized beams [1, 2, 3, 4, 5, 6]. Such beams are important to applications in fields such as nanomanipulation [7 8], biosensing [9], or quantum optics [10]. Recently, there has been a push to create angular momentum carrying light fields at the nanoscale [11], which would allow on-chip applications in the aforementioned fields.

At the nanoscale, properties of a light field such as the amount of angular momentum that they carry can be local quantities. That is, unlike in the far-field where the entire beam can carry angular momentum, in the near field distinct regions can have angular momentum while the entire distribution is neutral [12 13]. In the near field, regions with local angular momentum are often associated with optical singularities, either phase or polarization singularities in the cases of orbital- or spin-angular momentum, respectively. And, since near-fields are largely controlled by geometry, it is possible to design and fabricate structures, such as photonic crystal waveguides [12] or slits [14], whose nanoscopic light fields contain optical singularities.

Here, we introduce a new system where optical singularities can be found, namely a subwavelength hole on a metallic film as it scatters surface plasmon polaritons (SPPs). Unlike previous plasmonic systems whose fields are known to contain singularities [14], in our case we expect that the optical singularities will be found in the plane of the film. Our calculations do, in fact, reveal a plethora of both phase and polarization singularities in this plane, and we discuss their properties. We control the position of the singularities relative to the hole by tuning the size of either the incident SPP beam or the hole. Lastly, we show preliminary polarization- and phase-resolved near-field measurements of the scattering of SPPs from a subwavelength hole on a gold film, in which we observe polarization singularities.

2. Plasmonic scattering and phase singularities

The scattering of light from plasmonic nanostructures such as subwavelength holes results in complex electric field distributions [15, 16]. As these field distributions in the neighborhood of the hole are highly structured we can be hopeful that they might contain optical singularities [17,18]. The complexity of the field distribution arises from the fact that these distributions are composed of two different, interfering surface waves: the incident SPP beam, $\boldsymbol{E}^{in}$, and the scattered SPP, $\boldsymbol{E}^{s}$. For our situation of a SPP beam scattering from a hole in a gold film, the incident beam is simply a Gaussian SPP [15], while the scattered SPP wave can be written as [16]

$$\boldsymbol{E}^s(r) = -\frac{2\pi i\epsilon e^{-iw_{sp}z}}{\sqrt{1+\epsilon}(1-\epsilon)}\left[k_0^2\kappa_{sp}H_1^{(1)}(\kappa_{sp}r')cos\varphi m_y + ik_0\kappa_{sp}^2H_0^{(1)}(\kappa_{sp}r')p_z\right]\left(\hat{\boldsymbol{r}} - \frac{\kappa_{sp}}{w_{sp}}\hat{\boldsymbol{z}}\right). \qquad (1)$$

Here, $\kappa_{sp} = k_0\sqrt{(\epsilon+1)/\epsilon}$ and $w_{sp} = -k_0\sqrt{(\epsilon+1)}$ are the in-plane and out-of-plane components of the SPP wavevector, where $k_0 = 2\pi/\lambda$ is the free-space wavevector of light of wavelength λ and ϵ is the dielectric constant of gold. Further, in (1), $H_m^{(1)}$ are Hankel functions, $r' = \sqrt{(x-x_0)^2+(y-y_0)^2}$ corresponds to the displacement from the hole position $\boldsymbol{r}_0 = (x_0, y_0)$, $\hat{\boldsymbol{r}} = (cos\varphi\hat{\boldsymbol{x}}, sin\varphi\hat{\boldsymbol{y}})$, and φ is the angle from $\hat{\boldsymbol{x}}$ towards $\hat{\boldsymbol{y}}$. Finally, from (1) it is clear that the two dipoles that dominate the plasmonic response of the hole are the in-plane magnetic dipole m_y and the out-of-plane electric dipole p_z.

As sketched in figure 1, the total field in the region surrounding the hole is the superposition of the incident and scattered field. That is, $\boldsymbol{E}^T = \boldsymbol{E}^{in} + \boldsymbol{E}^s$, where the scattered field is, in this model, radiated by the dipoles that are induced in the hole by the incident field. Due to the symmetry of our nanophotonic system, these dipoles are simply $p_z = \alpha_E E_z^{in}(r_0)$ and $m_y = \alpha_H H_y^{in}(r_0)$, where the polarizability $\alpha_{E(H)}$ that determines the response of the hole to the incident electric (magnetic) field has been calculated [16] and measured [15].

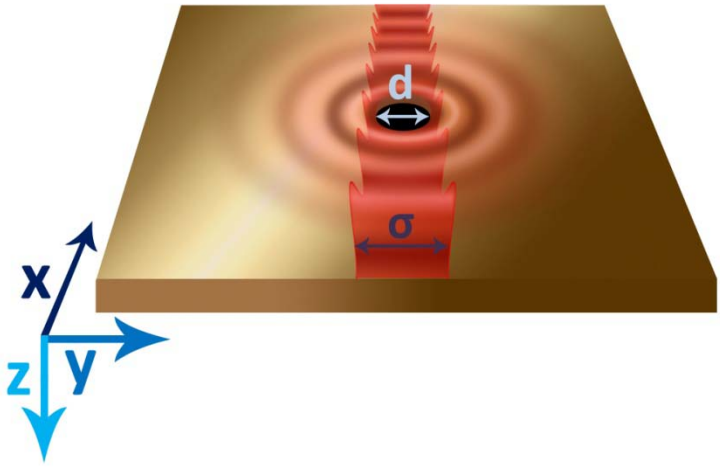

Figure 1. Schematic of our nanoplasmonic structure, including the coordinate system. An optically thick gold film supports a Gaussian SPP beam **(**σ FWHM), that scatters from a single subwavelength hole of diameter d.

Figure 2 shows an example of the calculated amplitude, $A(r)$, and phase, $\theta(r)$, of the vector components of $\boldsymbol{E}^{in}$ and $\boldsymbol{E}^s$ over an area of $40 \times 40\ \mu m^2$, at a height of 10 nm above the surface of the gold film. This calculation was performed for light with $\lambda = 1550$ nm, where $\epsilon = -155.1 + 11.3i$ [19]. In figure 2, $\boldsymbol{E}^{in}$ is a Gaussian SPP beam with a FWHM $\sigma = 5\ \mu m$ that propagates in the positive x direction and is centered around $y = 0$. As expected for a SPP beam, the strongest electric field

component is polarized out-of-plane, and hence E_z^{in} (figure 2e) is roughly 10 times larger than the longitudinal in-plane component E_x^{in} (figure 2a). Because $\boldsymbol{E}^{in}$ has a Gaussian shape, and is not a plane wave, we also find a non-zero distribution to the transverse electric field component E_y^{in} (figure 2c), which we expect would grow for beams with smaller widths.

The scattered field, shown in figure 2b, d, and f, is centered about the position of the hole at $\boldsymbol{r}_0 = (0,0)$. In these maps, the hole is taken to have a diameter of 800 nm, and the corresponding polarizabilities are $\alpha_E = -0.0448 + 0.0083i$ and $\alpha_H = 0.1301 + 0.1670i$ [16]. We observe a subtle asymmetry in the amplitude of the scattered field, with respect to the x axis, which arises due to the interference of the radiation by the electric and magnetic dipoles [15]. This directionality of the scattered field can be, in principle, controlled either through the polarizability of the hole (e.g. by changing the hole geometry), or the phases of the incident field (e.g. by changing $\boldsymbol{r}_0$ relative to the incident field, or using a different $\boldsymbol{E}^{in}$). In figure 2, we observe that the scattering is strongest in the forward direction.

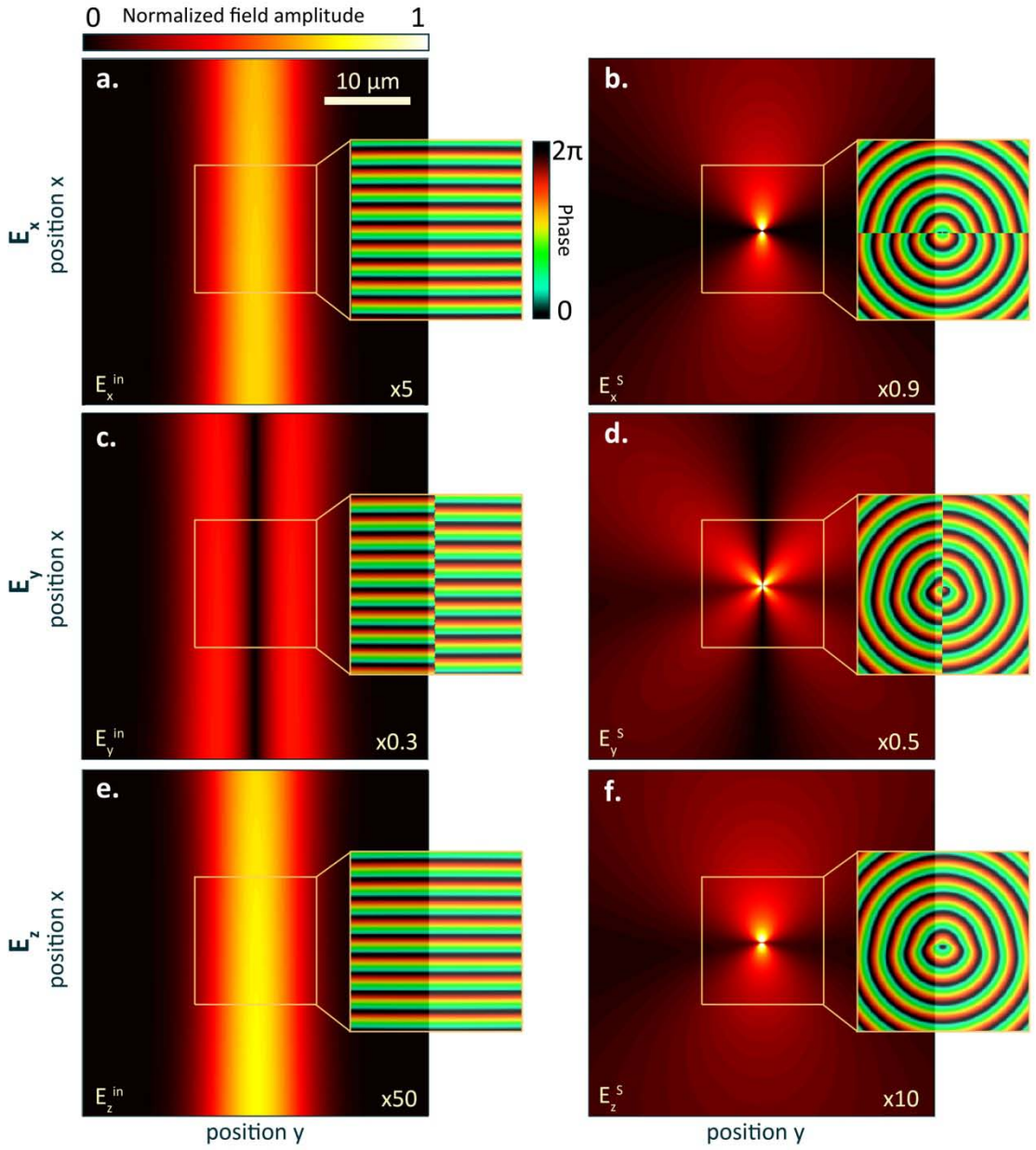

Figure 2. (a, c, e) Incident and (b, d, f) scattered electric field amplitude maps for a $\sigma = 5$ μm SPP beam scattering from an 800 nm hole. The beam propagates in the upwards direction, and the hole is located in the center of each map. The insets show the phase of each respective field component in a 15×15 μm^2 area that is centered on the hole. The relative amplitudes of the different components are given in the bottom right corner of each panel.

In addition to $A(r)$, we also present $\theta(r)$ for both the incident and scattered field, in the insets to figure 2. The phase of the incident field components (figure 2a, c, and e) increases monotonically in $\hat{\boldsymbol{x}}$, as

expected for a beam travelling in that direction. In contrast, the phase of the scattered field components (figure 2b, d, and f) grows with r', as expected for a circular wave radiating away from the hole.

We now look for phase singularities in the fields shown in figure 2. Phase singularities are points where $\theta(r)$ is undefined, and are generally found by looking for positions where different lines of constant phase intersect. Their intersection can only occur at points where the amplitude of the associated field is identically 0. The field maps shown in figure 2 contain no phase singularities, although some components (E_y^{in}, E_x^s, and E_y^s) do contain lines of undefined phase, known as wave disclinations, about which the phase flips. In our system, these disclinations are found on axes of symmetry, for example along $x = 0$ for E_y^{in} (figure 2c) or $y = 0$ for E_x^s (figure 2b).

While we find no phase singularities in the individual electric field components, such singularities are known to occur in systems where (two) different waves interfere [18]. In figure 3, we show both $A(r)$ and $\theta(r)$ for the three components of $\boldsymbol{E}^T$, made by adding the fields shown in figure 2. In the amplitude maps of $\boldsymbol{E}^T$ (figure 3a, d, and g) we observe parabolic fringes which arise from the interference of the incident SPP wave and the wave scattered by the hole. In fact, it is within these fringes that we can find positions where the incident and scattered waves have equal amplitudes and opposite phases, and hence the total field amplitude is 0.

Indeed, we find many intersection points of lines of different constant phase in the phase maps of $\boldsymbol{E}^T$ (figure 3b, e, and h), which we mark with symbols. We also mark these positions of undefined θ in the associated amplitude maps. We ensure that these points lie on position of zero amplitude by plotting

$$\boldsymbol{f}(r) = \log\left|\boldsymbol{A}^{in}(r) - \boldsymbol{A}^{s}(r)\right| + \log\left|\mathrm{mod}\left[\boldsymbol{\theta}^{in}(r) - \boldsymbol{\theta}^{s}(r), -\pi\right]\right|, \qquad (2)$$

in figure 3c, f, and i, and looking for points where $\boldsymbol{f}(r) = 0$. When $\boldsymbol{f}(r) = 0$, the amplitudes of the incident and scattered waves are equal (first term in (2)) and their phases are opposite (second term). That is, these points are indeed the phase singularities in the vector components of $\boldsymbol{E}^T$. It is interesting to note that the distributions of these singularities can greatly vary between components. In particular, the singularities in E_y^T are much closer to the hole than those of E_x^T and E_z^T. This difference is perhaps not unexpected, as the amplitude of E_y^{in} is smaller than that of the other two components, and hence the positions where the incident and scattered fields are equal occur at smaller r's.

Phase singularities are known to carry a topological charge, s, which denotes the number of times the phase of the electric field changes by 2π when traversing a loop around the singularity in the counter-clockwise direction. The singularities that we observe all carry a topological charge $s = \pm 1$, where s is constant within each quadrant of our maps, as we show in figure 2a, c, and e. For example, for E_y^T (figure 3d and e), $s = 1$ in the upper left and lower right quadrants, and $s = -1$ in the lower left and upper right

quadrant. That is, for every singularity with a positive topological charge there is one with a negative charge, such that the total topological charge of the plasmonic field is 0.

3. Polarization singularities

In addition to phase singularities, another class of singularities exists that occurs in light fields: the polarization singularity. In fact, there are different types of polarization singularities, which depend on what aspect of the polarization is singular. Although polarization singularities are properties of the total vector light field, and not of the individual components as can be the case for phase singularities it is possible to look for polarization singularities within a plane [12]. Here, we look for polarization singularities in the plane of our sample (the $x - y$ plane), where the electric field vector of the light, at any point, traces out an ellipse in time, as shown in figure 4a. Here, the polarization can be described by two variables: the ratio between the short and long axis, u/v, which is a measure of the ellipticity

$$\varepsilon(r) = \tan\left\{\sin^{-1}\left[\sin\left(2\psi(r)\right)\sin\left(\delta(r)\right)\right]/2\right\}. \quad (3)$$

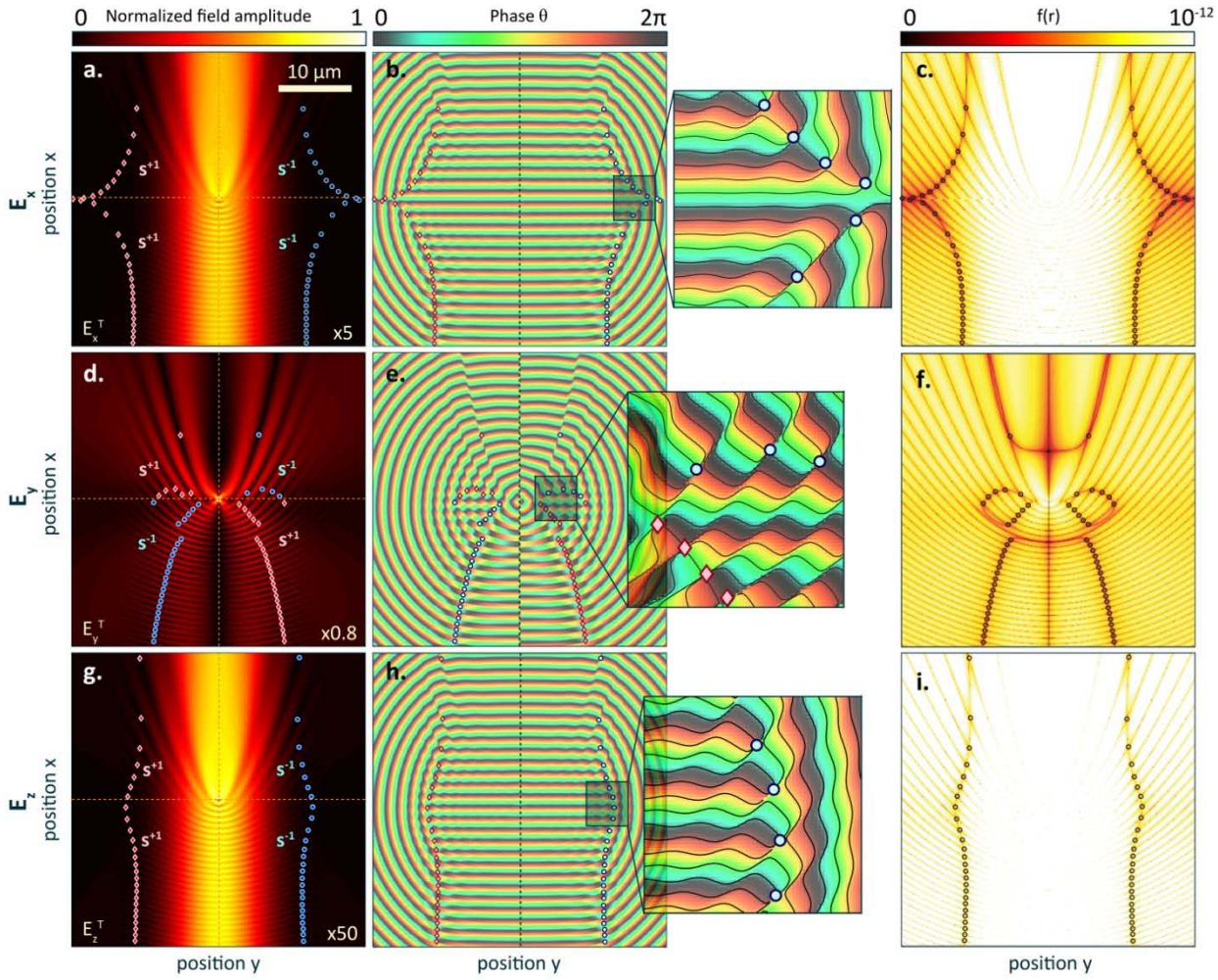

Figure 3. Electric field distributions that result when a 5 μm SPP beam scatters from a 800 nm wide hole. (a, d, g) The amplitude and (b, e, h) phase maps of $\boldsymbol{E^T}$ for the plasmonic scattering event, with the $s = 1(-1)$ phase singularities marked in solid red (blue) symbols. The relative amplitude of the different field components is shown in the bottom right of a, d, and g. (c, f, i) maps of $\boldsymbol{f}(r)$ (2) associated with (a, d, g) and (b, e, h), with the locations of the phase singularities marked with solid symbols. The singularities are found where $\boldsymbol{f}(r) = 0$, ensuring that they do occur when the amplitude of the associated field component (a, d, g) is also 0.

ε ranges from -1 to $+1$, with the sign corresponding to right- and left-circularly polarized light respectively. When $\varepsilon = 0$, the polarization of light is linear and the handedness in undetermined. The second parameter that describes the polarization of light is the orientation angle of the ellipse, which is given by

$$\alpha(r) = \left\{\tan^{-1}\left[\tan\left(2\psi(r)\right)\cos\left(\delta(r)\right)\right]/2\right\}, \quad (4)$$

which ranges from 0 to π. In these equations, $\psi(r) = \tan^{-1}\left[A_x(r)/A_y(r)\right]$ and $\delta = \theta_x(r) - \theta_y(r)$ are the amplitude ratio and the phase difference of E_x^T and E_y^T, respectively.

Polarization singularities are found at positions where either the handedness or the orientation of the polarization ellipse is undefined. We present the amplitude of the in-plane electric field $A_{xy}^T(r) = \sqrt{|E_x^T(r)|^2 + \left|E_y^T(r)\right|^2}$ in figure 4b, $\varepsilon(r)$ in figure 4c, and $\alpha(r)$ in figure 4d, using the field components shown in figure 3. We can immediately identify the singularities where the handedness of the light is undefined from the $\varepsilon(r)$ map, since these occur where the light is linear. As these singularities occur in lines they are known as L-lines, and we mark them in figure 4c (and figure 4d) with blue lines. Note that L-lines always separate regions where the light has opposite handedness.

The second type of polarization singularity, where the orientation of the polarization ellipse is undefined, occurs at a point where light is circularly polarized, and is therefore known as a C-point. In analogy to phase singularities, we find C-points by locating intersections of contour lines of constant α (known as isogyres, and are shown by black curves in our figures) in figure 4d. Additionally, we ensure that $\varepsilon = \pm 1$ at these locations. We show these C-points in figure 4 in symbols, where the colour and shape corresponds to the topological charge of the singularities. In our figures, a topological charge of $+1/2$ is shown in red diamonds, and a charge of $-1/2$ in blue circles. In analogy to phase singularities, we determine the topological charge of the C-points from figure 4c by tracing out the number of times the orientation of the polarization ellipse rotates by π as a loop around the C-point is transversed in a counter-clockwise direction. From figure 4 it is clear that in our plasmonic system we observe two regions that contain singularities, which roughly form stripes in the direction of propagation and can be found on either side of the hole. Further, within each strip, we find that the singularities come in pairs, where the inner singularity is negatively charged and the outer singularity is positively charged. As expected, an L-line runs in between each one of these singularity pairs (see figure 4c and d), and the total topological charge of the system is 0.

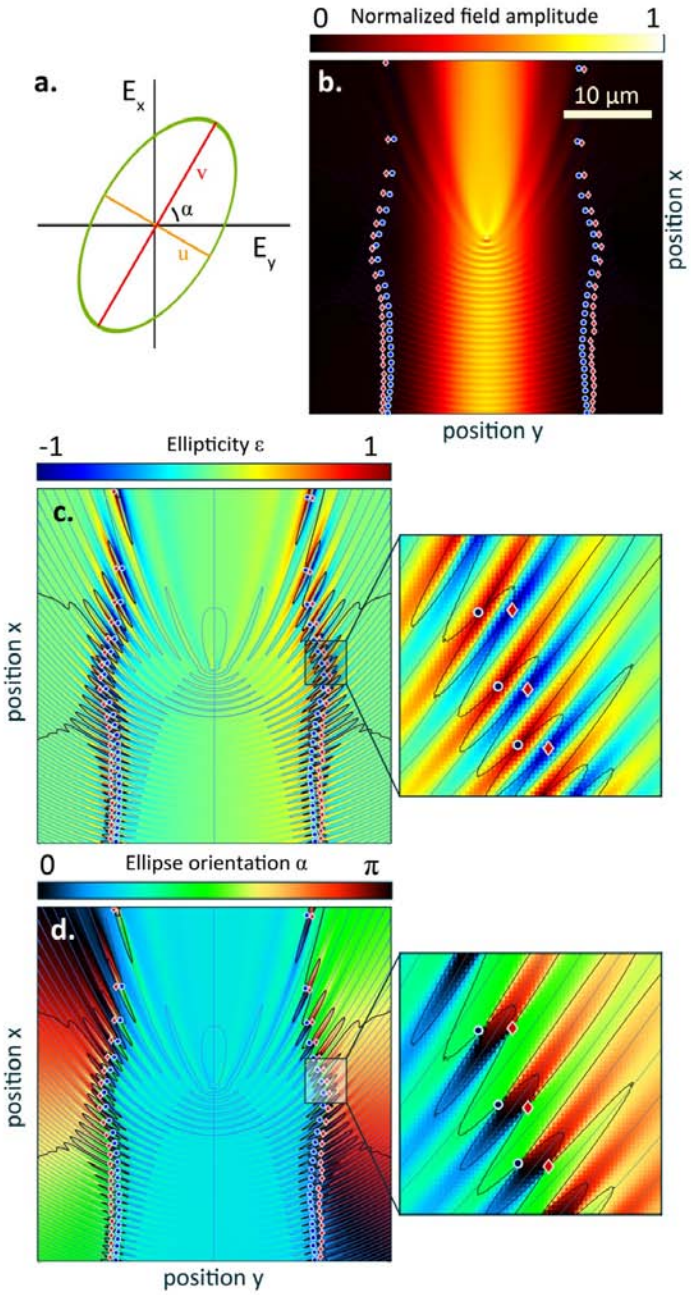

Figure 4. Polarization singularities in the plasmonic scattering event. (a) Schematic of the polarization ellipse traced out by the electric field vector in the plane of the gold film. (b) Amplitude map of the in-plane electric field of the scattering event. Polarization singularities with a topological charge of $1/2$ $(-1/2)$ are marked in solid red diamonds (blue circles). (c) Ellipticity and (d) orientation maps of the electric field distribution for the scattering event. In (c, d) L-lines $(\varepsilon = 0)$ are shown in light blue curves and isogyres (constant α) in black curves. The polarization singularities are again marked in solid symbols.

When a 5 μm SPP beam scatters from a 800 nm wide hole, our calculations show that the C-points are all located well away from $y = 0$ where the intensity is highest. Consequently, the field amplitude at a C-point is typically ≈ 2 to 25 times weaker than the incident field amplitude, at the hole. There are, however, two parameters in our model that can be varied, on which the position of the C-points might depend: the diameter of the hole, d, and the FWHM of the Gaussian beam σ, as shown in figure 1. By changing the size of the Gaussian SPP beam we change the rate at which the amplitude of $\boldsymbol{E}^{in}$ decreases with respect to its center at $y = 0$. Likewise, if we change the hole size, we change the efficiency with which it scatters light [16], and hence effectively change the magnitude of $\boldsymbol{E}^{s}$ relative to $\boldsymbol{E}^{in}$. That is, changing either, or both, of these parameters is expected to vary the positions where the interference of $\boldsymbol{E}^{s}$ and $\boldsymbol{E}^{in}$ creates C-points, and consequently the field amplitude at these singularities.

In figure 5 we show examples of $|\boldsymbol{E}^{T}|$ for several different hole and beam size combinations, in which we look to see if the locations of the C-points change. In figure 5a, where we again show $|\boldsymbol{E}^{T}|$ for a 5 μm FWHM SPP beam scattering from a 800 nm hole, we highlight 5 singularities that we will follow. As is seen in figure 5, when we increase d, while holding σ constant, then the singularities all shift towards $y = 0$. This movement occurs because the larger hole scatters light more efficiently [16], and hence the region where the amplitude of $\boldsymbol{E}^{s}$ is comparable to that of $\boldsymbol{E}^{in}$ shifts closer to the hole. We observe a similar behaviour, with the singularities shifting in towards $y = 0$, if we decrease σ while holding d constant (figure 5c).

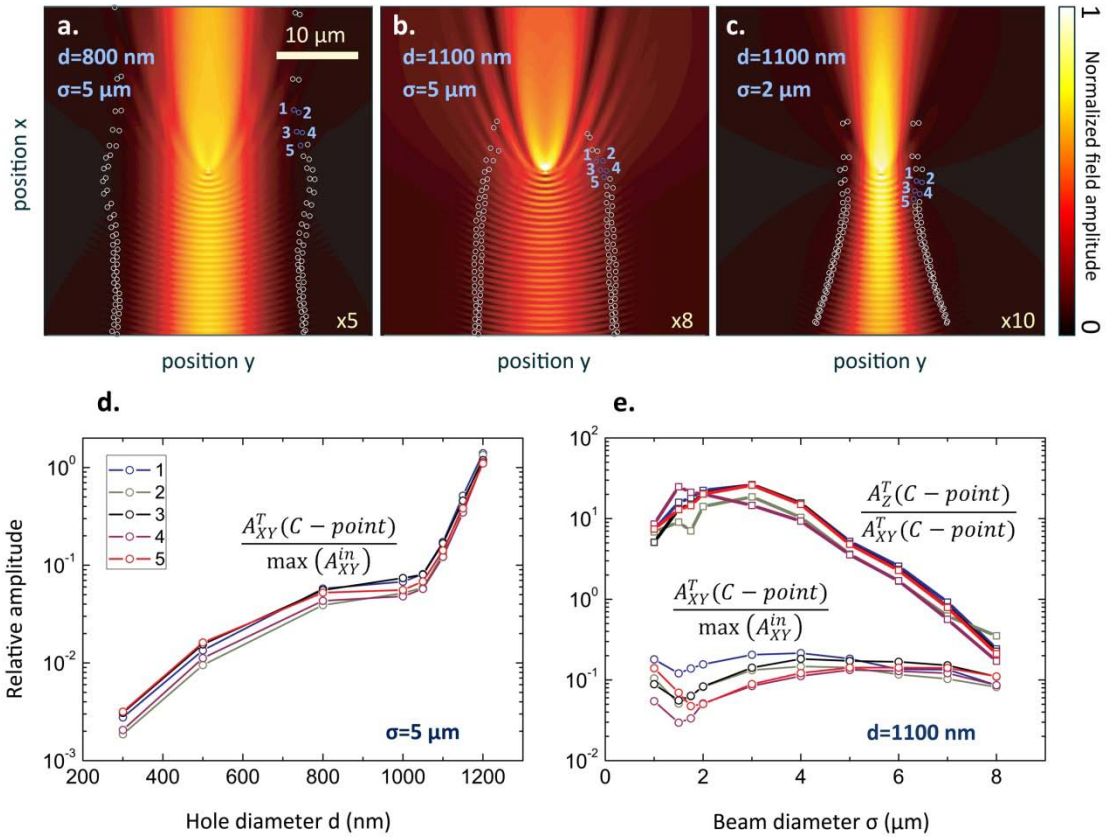

Figure 5. In-plane electric field amplitude maps for (a) a 5 μm SPP beam scattering from an 800 nm hole, (b) a 5 μm SPP beam scattering from an 1100 nm hole, and (c) 2 μm SPP beam scattering from an 800 nm hole. The locations of C-points in these maps are shown with white open circles, with 5 C-points shown in blue open circles and numbered, to help the reader observe how their positions depend on d and σ. The field amplitudes at the positions of the 5 C-points marked in (a, b, and c), normalized to the maximum of the incident in-plane field amplitude, as a function of (d) hole diameter and (e) beam diameter. The thick lines in (d) also show the ratio of the in-plane to out-of-plane electric field amplitudes at the location of the C-points.

The question then remains, whether the shift of the C-points in y that we observed when changing σ or d, moves them to regions of higher field amplitude. Consequently, we vary these two parameters in a systematic way, and track A at the positions of the C-points, as they shift, and plot the results in figure 5d and e. As shown in figure 5d, when the hole diameter is increased from 300 nm to 1200 nm, the relative electric field amplitude at the positions of the C-points increases, changing by almost 3 orders of magnitude over this range of hole sizes. We then fix $d = 1100$ nm, near where the electric field amplitude at the C-points is the strongest, and vary the beam diameter from 1 μm to 8 μm FWHM. We present the

results in figure 5e, where we observe that increasing the beam diameter has almost no effect on the relative amplitude of the in-plane electric fields at the C-point position, even though the C-points are pushed away from the hole (compare figure 5c to figure 5a). Interestingly, we also observe that changing the beam diameter decreases the amplitude of the out-of-plane electric field component, A_z^T, relative to the in-plane amplitude, A_{xy}^T, at the position of the C-points (thick solid lines in figure 5e), in this case by almost 2 orders of magnitude over the range of beam sizes that we study. This suggests that it is possible to tune both the absolute amount of in-plane electric field amplitude that is present at the C-point, as well as the ratio of in-plane to out-of-plane amplitude. Since changing the hole size has a larger effect on the amplitude at the singularity location than changing the beam diameter, it is likely that the interplay between these two parameters will allow for the design of systems with large in-plane electric field amplitudes at the C-point locations with concurrent small out-of-plane amplitudes. Such a situation might be desirable, since it is in the in-plane electric field amplitude that we look for the C-points.

4. Near-field measurements

Having studied the existence and control of C-points with theoretical simulations of plasmonic scattering events, we now hunt for their existence in experimental near-field data. We look for these singularities in data taken from Ref.15, where SPPs were launched towards a single subwavelength hole of 875 nm perforated in a 200 nm thick gold film on a glass substrate. The plasmonic scattering event was then imaged with a home-built near-field scanning optical microscope, using a heterodyne detection scheme which allows us to measure both the amplitude and phase of the in-plane field components [20]. The field maps are measured at a height of 20 nm above the sample.

In figure 6 we show (a) $\left|\boldsymbol{E}_{xy}(r)\right|$, (b) $\varepsilon(r)$, and (c) $\alpha(r)$, which we extracted from the near-field measurements. The measured in-plane field amplitude (figure 6a) is qualitatively very similar to the calculated in-plane field amplitude (figure 4a). In both the experiments and simulations we observe a strong Gaussian beam overlaid with parabolic interference fringes. There are, however, some differences between the measured and simulated field maps, which preclude a good quantitative agreement. Most importantly, in the measurements the hole is not located at the center of the beam but, as can be seen in figure 6a, can be found a little to the left. This minor, relative movement of the hole with respect to the beam, results in both a change to the relative phases of the electric and magnetic dipoles that describe the plasmonic scattering event, and a significant shift to the interference fringes. It is therefore reasonable to expect that the positions where $\boldsymbol{E}^s$ and $\boldsymbol{E}^{in}$ interfere to create C-points might also change. Second, the measurements contain some unwanted signals, and noise, which are not included in the simulations. Most obviously, in the measurements we see non-parabolic interference fringes, for example diagonal fringes to the right of the beam or horizontal fringes along the incident Gaussian SPPs. We attribute these fringes

mainly to reflections that occur outside of the scan area, leading to additional surface waves. Yet, despite these discrepancies between our measurements and the calculations, we do see that important features in the calculated fields were reproduced in the measurements.

We search for the polarization singularities in the map of $\alpha(r)$ where, in agreement with the theory, we find multiple C-points where isogyres intersect. As was the case in the calculations, the C-points observed in our measurements are distributed in columns along the propagation direction, both to the left and right of the incident beam. Unlike the theory, however, we observe many more rows of singularities, which we attribute to the presence of additional (surface) waves. Such additional waves can arise from extra reflections, as noted above, or due to imperfections during the excitation of the original SPP beam. In fact, the topological charges of all C-points, other than those in the innermost row, are randomly distributed between $s = \pm 1/2$. This random distribution of topological charge hints that these spurious singularities do, indeed, arise from noise and imperfections in the experiment. In contrast, all C-points in the innermost row, where the field amplitude is highest as is the signal-to-noise ratio, carry a topological charge of $s = -1/2$, in excellent agreement with the theory.

5. Conclusions

In conclusion, we find phase and polarization singularities in the electric field distributions that arise from the scattering of SPPs from single subwavelength holes in a gold film. These singularities are predicted by our theory and are also observed in near-field scanning optical microscopy measurements, although additional measurements are required for a quantitative comparison to be possible. We find that both the phase and polarization singularities are only found when both the incident and scattered waves are present and can interfere. Moreover, we show how by controlling the relative strengths of the incident and scattered waves, we can tune the position of the singularities, and even increase the field amplitude at the position of the C-points by 3 orders of magnitude. Because this control over the C-points is achievable by changing easily accessible parameters of the system, such as the hole size or incident beam diameter, we expect that our results will have importance to future on-chip applications requiring structured light fields.

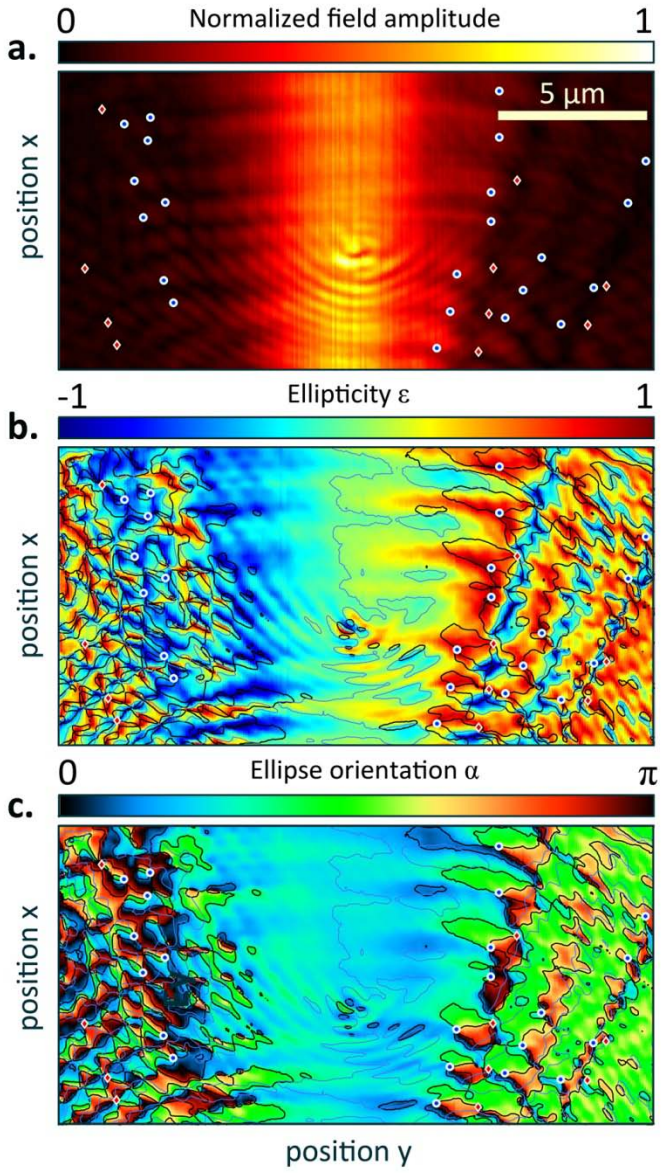

Figure 6. Near-field scanning optical microscopy measurements of the scattering of SPPs from a 875 nm hole. Maps of (a) the in-plane electric field amplitude, (b) ellipticity, and (c) ellipse orientation related to this scattering event. In all maps we mark C-points with symbols, using blue circles (red diamonds) for those with a topological charge of $-1/2$ $(1/2)$. In (b) and (c), L-lines are shown in thin light blue curves and isogyres in thick black curves.

Acknowledgements

The authors thank B. le Feber, R. van der Wel and A. Opheij for their insights and help in preparing this manuscript. This work is supported by the NQO program and the research program of the Stichting voor Fundamenteel Onderzoek der Materie (FOM), which is financially supported by the Nederlandse

organisatie voor Wetenschappelijk Onderzoek (NWO). Part of this work has been funded by the project "SPANGL4Q", which acknowledges the financial support of the Future and Emerging Technologies (FET) programme within the Seventh Framework Programme for Research of the European Commission, under FET-Open grant number: FP7-284743. L. K. acknowledges the financial support of the European Research Council.

References

[1] O'Neil A T, MacVicar I, Allen L and Padgett M J 2002 *Phys. Rev. Lett.* **88** 053601

[2] Berry M V and Dennis M R, 2001 *Proc. R. Soc. Lond. A* **457** 141

[3] Yao A M and Padgett M J 2011 *Adv. Opt. Photon.* **3**, 161-204

[4] Nye J F and Berry M V 1974 *Proc. R. Soc. A* **336** 165

[5] Shvartsman N and Freund I 1994 *Phys. Rev. Lett.* **72** 1008

[6] Nye J F 1983 *Proc. R. Soc. A* **387** 105

[7] He H, Friese M E J, Heckenberg N R, and Rubinsztein-Dunlop H 1995 *Phys. Rev. Lett.* **75** 826

[8] Schoonover R W and Visser T D 2006 *Opt. Express* **14** 5733

[9] Lavery M P J, Speirits F C, Barnett S M and Padgett M J 2013 *Science* **341** 537

[10] Cai X, Wang J, Strain M J, Johnson-Morris B, Zhu J, Sorel M, O'Brien J L, Thompson M G, Yu S 2012 *Science* **338** 363

[11] Andrews D L 2008 *Structured Light and its Applications* Academic Press

[12] Burresi M, Engelen R J P, Opheij A, van Oosten D, Mori D, Baba T and Kuipers L 2009 *Phys. Rev. Lett.* **102** 033902 1--4

[13] Flück E, Hammer M, Otter A M, Korterik J P, Kuipers L, and van Hulst N F 2003 *Journal of Lightwave Technology*, **21**(5) 1384

[14] Schouten H F, Visser T D, Gbur G, Lenstra D and Blok H 2004 *Phys. Rev. Lett.* **93** 173901

[15] Rotenberg N, Krijger T L, le Feber B, Spasenović M, García de Abajo F J and Kuipers L 2013 *Phys. Rev. B* **88** 241408 1-5

[16] Rotenberg N, Spasenović M, Krijger T L, le Feber B, García de Abajo F J and Kuipers L 2012 *Phys. Rev. Lett.* **108** 127402 1-5

[17] Nye J F 1999 *Natural Focusing and fine structure of light: caustics and wave dislocations* Bristol, Institute of Physics Publishing

[18] Balistreri M L M, Korterik J P Kuipers L and van Hulst N F 2000 *Phys. Rev. Lett.* **85** 294

[19] Johnson P B and Christy R W 1972 *Phys. Rev. B* **6** 4370

[20] Sandtke M , Engelen R J P, Schoenmaker H, Attema I, Dekker H, Cerjak I, Korterik J P, Segerink F B and Kuipers L 2008 *Rev. Sci.Instrum.* **79** 013704